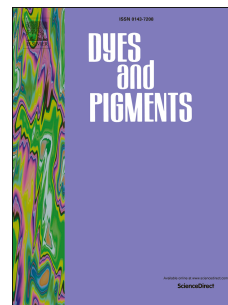


# Accepted Manuscript

Solvent boiling point affects the crystalline properties and performances of anthradithiophene-based devices

Tae Kyu An, Seong Jong Park, Eun Soo Ahn, Sang Hun Jang, Yebyeol Kim, Kyunghun Kim, Hyojung Cha, Yu Jin Kim, Se Hyun Kim, Chan Eon Park, Yun-Hi Kim



PII: S0143-7208(14)00424-0

DOI: [10.1016/j.dyepig.2014.10.027](https://doi.org/10.1016/j.dyepig.2014.10.027)

Reference: DYPI 4578

To appear in: *Dyes and Pigments*

Received Date: 27 September 2014

Revised Date: 29 October 2014

Accepted Date: 31 October 2014

Please cite this article as: An TK, Park SJ, Ahn ES, Jang SH, Kim Y, Kim K, Cha H, Kim YJ, Kim SH, Park CE, Kim Y-H, Solvent boiling point affects the crystalline properties and performances of anthradithiophene-based devices, *Dyes and Pigments* (2014), doi: 10.1016/j.dyepig.2014.10.027.

This is a PDF file of an unedited manuscript that has been accepted for publication. As a service to our customers we are providing this early version of the manuscript. The manuscript will undergo copyediting, typesetting, and review of the resulting proof before it is published in its final form. Please note that during the production process errors may be discovered which could affect the content, and all legal disclaimers that apply to the journal pertain.

# Solvent Boiling Point affects the Crystalline Properties and Performances of Anthradithiophene-based Devices

Tae Kyu An,<sup>a</sup> Seong Jong Park,<sup>b</sup> Eun Soo Ahn,<sup>b</sup> Sang Hun Jang,<sup>c</sup> Yebyeol Kim,<sup>a</sup> Kyunghun Kim,<sup>a</sup> Hyojung Cha,<sup>a</sup> Yu Jin Kim,<sup>a</sup> Se Hyun Kim,<sup>d</sup> Chan Eon Park,<sup>\*a</sup> and Yun-Hi Kim<sup>\*b</sup>

<sup>a</sup>POSTECH Organic Electronics Laboratory, Polymer Research Institute, Department of Chemical Engineering, Pohang University of Science and Technology, Pohang 790-784, Republic of Korea

<sup>b</sup>Department of Chemistry & Research Institute of Natural Science, Gyeongsang National University, Jinju 660-701, Republic of Korea

<sup>c</sup>School of Materials Science & Engineering and Engineering Research Institute (ERI), Gyeongsang National University, Jin-ju 660-701, Republic of Korea

<sup>d</sup>Department of Nano, Medical and Polymer Materials, Yeungnam University, Gyeongsan 712-749, Republic of Korea

\*Corresponding Author

Prof. Chan Eon Park E-mail: cep@postech.ac.kr

Prof. Yun-Hi Kim E-mail: ykim@gnu.ac.kr

Keywords: Organic field-effect transistor (OFET), Anthradithiophene (ADT), X-ray diffraction (XRD), crystallinity, boiling point

## Abstract

We investigated the effects of the solvent boiling point on organic field-effect transistor (OFET) device performances in devices prepared using two newly synthesized anthradithiophene derivatives: 9,10-di(4'-pentylphenylethynyl)-anthra[2,3-b:6,7-b']dithiophene (DPPEADT) and 9,10-bis(9,9'-dimethyl-fluorene-2-ylethynyl)-anthra[2,3-b:6,7-b']dithiophene (DFEADT). DPPEADT exhibited a distinct crystalline morphology whereas DFEADT was amorphous. We characterized the relationship between the molecular

structures, film morphologies, and OFET device performances in devices prepared using solvents having one of three different boiling points (chlorobenzene, 1,2-dichlorobenzene, and 1,2,4-trichlorobenzene). 1,2,4-Trichlorobenzene, which provided the highest boiling point among the solvents tested and acted as a good solvent for DPPEADT, significantly improved the field effect mobilities of DPPEADT devices up to  $0.16 \text{ cm}^2/\text{Vs}$  by enhancing the crystallinity of the film. OFETs based on amorphous DFEADT films prepared using the three solvents did not provide enhanced electrical performances. The differences between the transistor performances were attributed to the degree of  $\pi$ -overlap, the molecular structures, and the morphological properties of the films.

## 1. Introduction

Over the past two decades, organic semiconductors have received significant attention as components in organic field-effect transistors (OFETs) [1, 2], organic light emitting diodes (OLEDs) [3, 4], organic photovoltaic cells (OPVs) [5, 6], and organic photodetectors (OPDs) [7, 8] for potential use in flexible, inexpensive, and large-area electronics applications [9, 10]. A variety of organic semiconductor materials have been developed, and their electrochemical properties have been investigated in an effort to realize more efficient organic electronic device performances. Solution-processable small molecule semiconductors have been most extensively studied because their synthesis, purification, and structural modifications are relatively easy and they provide low batch-to-batch variability [11, 12].

Anthradithiophene (ADT) derivatives are promising candidates for use in organic semiconductors because these derivatives are highly solubility in common organic solvents and they display excellent charge carrier mobilities [13]. ADT derivatives tend to resist oxidation to a greater extent than pentacene, yielding devices with good long-term stability properties [14]. Research efforts geared toward developing high-performance OFETs based

on ADT derivatives have focused on novel design strategies that enhance the molecular ordering in a film [15, 16]. The electrical properties of ADT derivatives may be enhanced by optimizing the device preparation protocols, including selecting a suitable solvent [17] that yields a high ADT solubility or introducing dielectric surface treatments [18] that induce the formation of favorable crystalline structures.

Previous studies found that high boiling point solvents produced highly crystalline semiconductor thin films because the longer drying times permitted self-organization among the organic semiconductor molecules, thereby increasing the field effect mobility ( $\mu_{\text{FET}}$ ) in the corresponding OFETs [19]. Siringhaus et al. reported enhanced  $\mu_{\text{FET}}$  values for OFETs prepared with poly(3-hexylthiophene) as the semiconductor and 1,2,4-trichlorobenzene as the solvent. Seo et al. improved the performances of a 6,13-bis(triisopropylsilylethynyl) pentacene OFET by introducing solvent additives with high boiling points (b.p.) [20, 21]. Unfortunately, the surface tensions of high b.p. solvents tend to be high, whereas the surface energy of the substrate tends to be low. Organic semiconductor films, therefore, tend to dewet during film formation due to the large difference between the surface energies of the solvent and the dielectric surface [22, 23].

The gate dielectric surfaces of OFETs are typically modified by introducing hydrophobic oligomeric or polymer materials that minimize the formation of charge carrier traps [24]. A variety of gate dielectric treatment layers have been tested thus far. Hydrophobic self-assembled monolayers (SAMs) are commonly used on polar dielectric layers because they can efficiently cover the underlying polar dielectric functionalities that act as charge carrier traps, and they can accompany epitaxial growth of organic semiconductor films to improve the values of  $\mu_{\text{FET}}$  [25, 26]. Despite the performance improvements obtained through the use of SAMs in OFETs [27, 28], the hydrophobicity of the SAM layer promotes dewetting of the solution-processed material from the surface [22,

23]. Only solvents with a low b.p. can be used during the solution-processed film formation steps on a hydrophobic SAM-treated substrate [29-31]. The electrical performances of OFETs may be optimized through the use of high b.p. solvent combinations and hydrophobic dielectric surface treatments.

The challenges associated with pairing appropriate solvents and surface treatments were overcome in this research by introducing an ultrathin polymer brush layer. Polymer brushes can produce chemically stable molecular nanolayer films at a dielectric surface. The hydrophobicity of the polymer brushes can be selected so as to overcome the dewetting problems associated with high boiling point solvents. For these reasons, polymer brush-based OFETs provide  $\mu_{\text{FET}}$  values that are comparable to those obtained from SAM-treated dielectric systems [32, 33].

The present study describes a strategy for optimizing the self-organization of newly synthesized ADT derivatives by introducing high b.p. solvents and hydrophobic chlorosilane-terminated polystyrene (PS-brush) surface treatments [33]. Chlorobenzene (CB), 1,2-dichlorobenzene (DCB), and 1,2,4-trichlorobenzene (TCB) were used as solvents for the ADT semiconductor derivatives. The b.p. values of CB, DCB, and TCB were 131, 180.5, and 214.4°C. The newly synthesized 9,10-di(4'-pentylphenylethynyl)-anthra[2,3-b:6,7-b']dithiophene (DPPEADT) and 9,10-bi(9',9'-dimethyl-fluoren-2-ylethynyl)-anthra[2,3-b:6,7-b']dithiophene (DFEADT) were used to form the semiconducting layer (**Scheme 1**). In DPPEADT, the presence of extensively conjugated phenyl groups connected to the pentyl group might be expected to further promote the self-assembly of the ADT moiety because the phenyl groups were located on the symmetrically perpendicular to the ADT unit [14]. By contrast, fluorine moieties in DFEADT generated steric hindrance at the periphery of the molecule, leading to the formation of an amorphous morphology [14, 34, 35]. DPPEADT-based OFETs exhibit better  $\mu_{\text{FET}}$  values when prepared using high b.p. solvents, whereas the

DFEADT devices yielded  $\mu_{\text{FET}}$  values that were insensitive to the solvent b.p. These results suggested that the OFET performance is only sensitive to the solvent b.p. in the case of crystalline ADT derivatives because the longer drying times due to the higher b.p facilitate the formation of favorable molecular packing structures. Clear correlations between the OFET performances and the crystalline structures of the ADT derivative thin films were revealed using several structural analysis techniques.

## 2. Results and Discussion

### 2.1 Synthesis, thermal and electrochemical analysis

The synthetic schemes used to prepare DPPEADT and DFEADT are depicted in **Scheme 1**. The ADT derivatives were prepared by an aldol condensation, nucleophilic addition, and reduction. The structures of DPPEADT and DFEADT were confirmed by H-NMR and Mass spectroscopies. The ADT derivatives displayed good solubilities due to the presence of bulky aryl substituents. The thermal stabilities of the ADT derivatives were examined using thermogravimetric analysis (TGA) and by collecting differential scanning calorimetry (DSC) thermograms. The DPPEADT and DFEADT films displayed excellent thermal stabilities, with decomposition temperatures of 429°C and 435°C, respectively. The DSC thermograms showed revealed that DPPEADT and DFEADT did not undergo transitions during heating to 250°C. The highest occupied molecular orbital (HOMO) levels of DPPEADT and DFEADT were calculated based on the oxidation onset, as measured using cyclic voltammetry (CV), and were shown to be -5.18 eV and -5.22 eV, respectively. The optical band gaps of DPPEADT and DFEADT were 2.07 eV and 2.03 eV, respectively, obtained from the onset of the UV absorption bands. The HOMO levels were characterized by theoretically calculating the lowest unoccupied molecular orbital (LUMO) and the electron density distributions using density function theory (DFT) methods with the hybrid

B3LYP functional in Gaussian 09. The optimized geometries and electron density distributions of the HOMO and LUMO of DPPEADT and DFEADT are shown in **Fig. S1**. In both materials, the HOMOs were localized along the ADT unit, and the LUMOs were localized along the extended aromatic side units as well as the ADT unit. The DFT-computed HOMO/LUMO values followed similar trends in the electrochemical and optical analyses.

## 2.2 UV–vis absorption spectroscopy

The optical absorption spectra of the two ADT derivatives were obtained in the solution and film states, as shown in **Fig. 1**. The absorption maxima ( $\lambda_{\max}$ ) of the solution and thin film spectra are reported in **Table 1**. A comparison of the peaks present in the DPPEADT and DFEADT UV-vis spectra in dilute solution form revealed that the maximum peak of DPPEADT occurred at lower wavelengths than the corresponding peak of DFEADT. These results were consistent with the long conjugated segment length in DFEADT, which lowered the  $\pi \rightarrow \pi^*$  transition energy gap [36, 37]. We discovered that the absorption peaks of the ADT derivatives in the thin film state were red-shifted relative to those observed in the solution state (**Fig. 1** and **Table 1**). The magnitude of the DFEADT absorption peak red shift was smaller than that observed in DPPEADT. The shift in the peak positions indicated the extent of molecular packing in the film state. A structural analysis based on the UV-vis absorption spectrum revealed that the molecular ordering within the DPPEADT thin film was greater than the molecular ordering in the DFEADT thin film. These results were consistent with the X-ray diffraction (XRD) results, as discussed in the following section.

## 2.3 Thin-Film Structure and Morphology

**Figure 2** shows the XRD patterns obtained from ADT derivative thin films deposited using different solvents onto PS-brush-treated Si/SiO<sub>2</sub> substrates via spin-coating. The

DPPEADT films prepared from CB and DCB showed two diffraction peaks along the out-of-plane direction at  $2\theta = 3.90$  and  $7.72^\circ$  with an interlayer distance of  $15.8 \text{ \AA}$ . The observed interlayer distance was shorter than the calculated width of the full side chain ( $29 \text{ \AA}$ , Supporting Information **Fig. S2**), suggesting that the side chains were either bent or interdigitated with the side chains of the adjacent DPPEADT molecules. The out-of-plane scattering profiles of the DPPEADT film prepared from TCB showed more well-defined diffraction patterns, including a 3rd-order peak, compared to the DPPEADT films prepared from CB and DCB [38]. The first peak width measured in the film prepared from TCB was slightly narrower than the corresponding peak width in films prepared from CB and DCB, although the interlayer distances were indistinguishable. These studies indicated that the DPPEADT film prepared from TCB formed more extensive long-range intermolecular interactions or a higher degree of molecular ordering than the DPPEADT films prepared from CB and DCB [39]. The in-plane scattering profiles of the DPPEADT films (**Fig. 2(b)**) revealed (010) peaks at  $2\theta = 16.7^\circ$ , which corresponded to a  $\pi$ - $\pi$  stacking distance of  $3.69 \text{ \AA}$ . The scattering peak at  $2\theta = 13.2^\circ$  provided an estimate for the d-spacing of  $4.66 \text{ \AA}$ . This distance probably corresponded to the inter-alkyl side chain distance (**Fig. 3**). The DPPEADT film diffraction pattern intensity along the in-plane direction increased as the solvent b.p. increased. The XRD data revealed that the DPPEADT films prepared from TCB achieved a higher degree of  $\pi$ -overlap than the DPPEADT films prepared from CB and DCB. The degree of  $\pi$ -overlap and the molecular ordering among molecules along the in-plane direction are important features of high-performance OFETs because charge carriers in an organic medium move among  $\pi$ -overlapping regions along the in-plane direction [40, 41]. The development of molecular ordering along the in-plane direction strengthened the  $\pi$ -orbital overlap in the semiconductor film, thereby improving charge carrier transport. As shown in **Fig. 2(c)** and **2(d)**, no scattering peaks were observed in any of the DFEADT film states. These findings

indicated that the DFEADT films were amorphous [42, 43].

Atomic force microscopy (AFM) images were collected to characterize the surface morphologies of the DPPEADT and DFEADT films, as shown in **Fig. 4**. The DPPEADT film prepared from the CB solution included discontinuous large defects on the film, which tended to interrupt hole transport because the grain boundaries usually promoted trap formation and limited charge carrier hopping between crystal domains [44]. As the solvent b.p. increased, the morphologies of the DPPEADT films prepared from DCB and TCB exhibited terrace-like crystalline structures that revealed several continuous layers and partial layer-by-layer growth. The DFEADT films displayed a featureless and smooth morphology. The DFEADT film morphologies did not depend on the solvent, and the solvent did not extensively alter the structure of the amorphous film.

## 2.4 FET Behavior

The effects of the solvent b.p. on the charge transport characteristics of each ADT derivative were investigated by fabricating OFETs using spin-coating techniques, as shown in **Fig. 5**. **Figure 6** shows that the OFET devices prepared using the ADT derivatives displayed typical p-channel responses in the saturation regime. The electrical parameters of the OFETs are summarized in **Table 2**. The values of  $\mu_{\text{FET}}$  for the DPPEADT-based OFETs depended on the solvent b.p.: the TCB device yielded a  $\mu_{\text{FET}}$  value up to  $0.16 \text{ cm}^2/\text{Vs}$ , about one order of magnitude greater than the value obtained from CB ( $0.018 \text{ cm}^2/\text{Vs}$ ). The high  $\mu_{\text{FET}}$  values obtained from TCB-based OFETs were attributed to a high degree of crystallinity and a highly overlapping surface morphology in the DPPEADT film developed in the presence of a high b.p. solvent. The amorphous DPPEADT OFETs did not display better electrical characteristics as the solvent b.p. was increased. The DFEADT-based OFETs provided constant  $\mu_{\text{FET}}$  values of  $4 \times 10^{-6} \text{ cm}^2/\text{Vs}$ .

OFET performances are significantly affected by the molecular ordering, crystallinity, and morphology of the organic semiconductor thin film. Structural and morphological analyses based on the UV–visible absorption spectrum, XRD studies, and AFM measurements revealed differences between the OFET behaviors. The effects of the high boiling point solvents were found to control the crystalline characteristics of the organic semiconductors. Solvents with a high b.p. were indeed capable of improving the self-organization and, therefore, the hole transport in the crystalline DPPEADT film due to the longer solvent evaporation time. The amorphous DFEADT film, as shown in **Figs. 2(c)** and **2(d)** and **Figs. 4(d–f)**, did not display morphological or crystalline characteristic changes upon the introduction of a high boiling point solvent. Methods of tuning the solvent evaporation rate as a means for controlling the crystallinity of the semiconductor thin film have been described previously [45].

The effects of the film crystallinity on the electrical properties of DPPEADT OFETs were investigated by measuring the hysteresis behavior, defined as the difference between the off-to-on and on-to-off swept transfer curves. As shown in **Fig. 7**, the DPPEADT-based OFETs prepared from CB, DCB, and TCB displayed negligible hysteresis under N<sub>2</sub>; however, each sample exhibited different degrees of crystallinity and corresponding  $\mu_{\text{FET}}$  values, depending on the solvent b.p. Many OFET systems display hysteresis properties that are commonly attributed to the presence of polar dielectric functional groups (such as hydroxyl groups), water molecules, or oxygen molecules at the semiconductor/dielectric interface. Some systems appear to display hysteresis properties as a result of the semiconductor morphology [46–48]. In our system, the polar dielectric functional group coverage (the PS-brushes) and the inert operation conditions minimized hysteresis-causing factors [19, 33]. The differences in the DPPEADT crystalline morphology, therefore, influenced the charge transport properties rather than the hysteresis.

### 3. Conclusions

The relationship between the performances of solution-processed organic transistor device and the crystalline characteristics of the small molecule films prepared using solvents with a variety of boiling points was investigated by designing and synthesizing two ADT-based small semiconducting molecules. The DPPEADT films displayed crystalline characteristics whereas the DFEADT films showed highly amorphous characteristics. The presence of a PS-brush SAM increased the wettability of the film on the SiO<sub>2</sub> substrate during film formation from common high boiling point organic solvents. The introduction of high boiling point solvents enhanced the molecular ordering in the crystalline DPPEADT films by facilitating the formation of extended  $\pi$ - $\pi$  conjugated systems, thereby dramatically increasing the field-effect mobilities in the OFETs. Controlling the morphology of the DPPEADT film through the use of organic solvents with different boiling points produced transistors with a mobility of 0.16 cm<sup>2</sup>/Vs. The device hysteresis behavior depended on the degree of crystallinity. The effects of the high boiling point solvent were only observed in the crystalline semiconductor film, which was capable of improving its molecular packing structure when allowed a longer crystallization period. On the other hand, the high boiling point solvent did not significantly alter the structures or morphologies of the highly amorphous DFEADT films. The appropriate combination of high boiling point solvents and surface treatments to produce a crystalline semiconductor film increased the value of  $\mu_{\text{FET}}$ .

### 4. Experimental

All reagents were obtained from commercial sources and were used without further purification. Toluene, tetrahydrofuran (THF), chlorobenzene (CB), and 1,2-dichloromethane (DCM) were

purchased from Aldrich and were purified by passage under a N<sub>2</sub> atmosphere. 1-Ethynyl-4-pentylbenzene was purchased from Aldrich.

#### *Measurements*

The <sup>1</sup>H NMR spectra were recorded using an Avance-300 MHz spectrometer. Mass spectra were measured using a Jeol JMC-700 and GCmate2. The thermal analysis was performed on a TA 2050 TGA thermogravimetric analyzer under a nitrogen atmosphere. The samples were heated at 10°C/min. Differential scanning calorimetry was conducted under nitrogen on a TA instrument 2100 DSC. The samples were heated at 20°C/min from 0°C to 250°C. UV-vis absorption studies were carried out using a Perkin-Elmer LAMBDA-900 UV/VIS/IR spectrophotometer.

**Anthra[2,3-*b*:6,7-*b'*]dithiophene-5,11-dione.** Thiophene-2,3-dicarboxaldehyde (5 g, 35.7 mmol) was dissolved in EtOH (450 mL) in a 1 L round-bottom flask with a stir bar, followed by the addition of 2 g 1,4-cyclohexane dione (17.8 mmol). Upon the addition of a 15% KOH solution (20 mL), a precipitate began to form immediately. The mixture was stirred for an additional hour then filtered to yield 4.8 g (15 mmol, 84%) of quinone as a yellow powder. Mp: 380 -383 C, MS (EI): m/z 320 (M+).

**DPPEADT.** To an oven-dried 100 mL round-bottom flask equipped with a stir bar and cooled under N<sub>2</sub> were added 3.7 mL *n*-BuLi (9.36 mmol, 2.5 M solution in hexanes), followed by the dropwise addition of 1.82 mL 1-ethynyl-4-pentylbenzene (9.36 mmol). This mixture was stirred for 1 hr then hexanes (130 mL) and quinone (0.5 g, 1.56 mmol) were added. The mixture was heated at 60°C overnight. SnCl<sub>2</sub> (2 g, 10.92 mmol) in 10% HCl (5 mL) was added, and the mixture was stirred for 2 hr at 60°C. The solution was dried over MgSO<sub>4</sub> then loaded onto a thick pad of silica. The silica was rinsed with hexanes (500 mL), and the product was eluted using hexanes. Removal of the solvent yielded 0.49 g (0.78 mmol, 50%) of a violet powder. Recrystallization from hexanes yielded pure **DPPEADT** as a violet powder. <sup>1</sup>H-NMR (300 MHz, CDCl<sub>3</sub>) δ = 9.25 (d, 2H), 8.35 (d, 2H), 7.81–7.74

(m, 4H), 7.57–7.50 (m, 4H), 7.45 (d, 1H), 7.36–7.28 (m, 4H), 2.78 (t, 4 H,  $J = 7.58$  Hz), 1.72–1.57 (m, 4 H), 1.40–1.38 (m, 8 H), 0.95–0.94 (m, 6H),  $^{13}\text{C-NMR}$  (500 MHz,  $\text{CDCl}_3$ )  $\delta$  144.1, 140.0, 139.9, 139.4, 139.3, 132.4, 131.7, 129.8, 129.7, 129.6, 129.4, 128.7, 123.7, 121.2, 120.0, 104.0, 87.1, 36.0, 31.4, 29.7, 22.5, 14.0, MS (EI):  $m/z$  630 ( $\text{M}^+$ ).

**DFEADT.** To an oven-dried 100 mL round-bottom flask equipped with a stir bar and cooled under  $\text{N}_2$  were added 3.12 mL  $n\text{-BuLi}$  (7.8 mmol, 2.5 M solution in hexanes), followed by the dropwise addition of 1.7 mL 2-ethynyl-9,9-dimethyl-9H-fluorene (7.8 mmol). This mixture was stirred for 1 hr then hexanes (130 mL) and quinone (0.5 g, 1.56 mmol) were added. The mixture was heated at  $60^\circ\text{C}$  overnight.  $\text{SnCl}_2$  (2 g, 10.92 mmol) in 10% HCl (5 mL) was added, and the mixture was stirred for 2 hr at  $60^\circ\text{C}$ . The solution was dried over  $\text{MgSO}_4$  then loaded onto a thick pad of silica. The silica was rinsed with hexanes (500 mL), and the product was eluted using hexanes. Removal of the solvent yielded 0.4 g (0.55 mmol, 37%) of a violet powder. Recrystallization from hexanes yielded pure **DFEADT** as a violet powder.  $^1\text{H-NMR}$  (300 MHz,  $\text{CDCl}_3$ )  $\delta = 9.26$  (s, 4H), 8.08–8.06 (m, 4H), 7.97 (s, 2H), 7.92–7.90 (m, 3H), 7.87–7.83 (m, 2H), 7.55–7.54 (m, 2H), 7.47–7.28 (m, 9H), 1.68 (s, 12H),  $^{13}\text{C-NMR}$  (500 MHz,  $\text{CDCl}_3$ )  $\delta$  154.11, 153.96, 140.09, 139.58, 139.0, 138.5, 131.1, 129.8, 129.6, 129.5, 127.2, 126.7, 125.9, 123.8, 122.7, 121.9, 121.3, 120.6, 120.4, 120.2, 120.0, 117.4, 104.2, 87.4, 47.1, 27.1, MS (EI):  $m/z$  722 ( $\text{M}^+$ ).

#### *Fabrication and Characterization of the OFET Devices*

Top-contact OFETs were fabricated on a common gate of highly n-doped silicon with a 300 nm thick thermally grown  $\text{SiO}_2$  dielectric layer. The PS-brush ( $M_w = 9$  k) solution was spin-coated onto the substrates in ambient air, and the resulting films were annealed at  $110^\circ\text{C}$  for 1 h, as described previously [33]. Unreacted residues of the PS-brush were rinsed with excess toluene and then sonicated in a toluene bath for 3 min. Solutions of the organic semiconductors were spin-coated at 2000 rpm from 0.7 wt% solutions to form thin films with

a nominal thickness of 40–50 nm, as confirmed using a surface profiler (Alpha Step 500, Tencor). Gold source and drain electrodes were evaporated on top of the semiconductor layers (100 nm). For all measurements, we used channel lengths ( $L$ ) of 160  $\mu\text{m}$  and channel widths ( $W$ ) of 1600  $\mu\text{m}$ . The electrical characteristics of the FETs were measured in air using Keithley 2400 and 236 source/measure units. Field-effect mobilities were extracted in the saturation regime from the slope of the source–drain current. 1D XRD studies were performed at the Pohang Accelerator Laboratory (beamline 5A).

### **Acknowledgment.**

Tae Kyu An and Seong Jong Park equally contributed to be the first authors to this work. This research was financially supported by the National Research Foundation of Korea (NRF), funded by the Ministry of Education, Science and Technology (2012R1A2A2A06047047 and NRF-2014R1A2A1A05004993). This work was also supported by the Center for Advanced Soft-Electronics funded by the Ministry of Science, ICT and Future Planning as Global Frontier Project (2012M3A6A5055225 and 2011-0031639).

## References

- [1] Kim G, Kang S-J, Dutta GK, Han Y-K, Shin TJ, Noh Y-Y, et al. A Thienoisindigo-Naphthalene Polymer with Ultrahigh Mobility of  $14.4 \text{ cm}^2/\text{V}\cdot\text{s}$  That Substantially Exceeds Benchmark Values for Amorphous Silicon Semiconductors. *J Am Chem Soc.* 2014;136(26):9477-83.
- [2] Kang I, Yun H-J, Chung DS, Kwon S-K, Kim Y-H. Record High Hole Mobility in Polymer Semiconductors via Side-Chain Engineering. *J Am Chem Soc.* 2013;135(40):14896-9.
- [3] Farinola GM, Ragni R. Electroluminescent materials for white organic light emitting diodes. *Chem Soc Rev.* 2011;40(7):3467-82.
- [4] So KH, Kim R, Park H, Kang I, Thangaraju K, Park YS, et al. Synthesis and characterization of a new iridium(III) complex with bulky trimethylsilylylene and applications for efficient yellow-green emitting phosphorescent organic light emitting diodes. *Dyes Pigm.* 2012;92(1):603-9.
- [5] Cha H, Chung DS, Bae SY, Lee M-J, An TK, Hwang J, et al. Complementary Absorbing Star-Shaped Small Molecules for the Preparation of Ternary Cascade Energy Structures in Organic Photovoltaic Cells. *Adv Funct Mater.* 2013;23(12):1556-65.
- [6] Tamayo AB, Dang X-D, Walker B, Seo J, Kent T, Nguyen T-Q. A low band gap, solution processable oligothiophene with a dialkylated diketopyrrolopyrrole chromophore for use in bulk heterojunction solar cells. *Appl Phys Lett.* 2009;94(10):103301.
- [7] An TK, Park CE, Chung DS. Polymer-nanocrystal hybrid photodetectors with planar heterojunctions designed strategically to yield a high photoconductive gain. *Appl Phys Lett.* 2013;102(19):193306.
- [8] Yiming W, Xiujuan Z, Huanhuan P, Xiwei Z, Yuping Z, Xiaozhen Z, et al. Large-area aligned growth of single-crystalline organic nanowire arrays for high-performance photodetectors. *Nanotechnology.* 2013;24(35):355201.
- [9] Kang B, Min H, Seo U, Lee J, Park N, Cho K, et al. Directly Drawn Organic Transistors by Capillary Pen: A New Facile Patterning Method using Capillary Action for Soluble Organic Materials. *Adv Mater.* 2013;25(30):4117-22.
- [10] Petritz A, Wolfberger A, Fian A, Krenn JR, Griesser T, Stadlober B. High performance p-type organic thin film transistors with an intrinsically photopatternable, ultrathin polymer dielectric layer. *Org Electron.* 2013;14(11):3070-82.
- [11] Ha J-j, Kim YJ, Park J-g, An TK, Kwon S-K, Park CE, et al. Thieno[3,4-c]pyrrole-4,6-

dione-Based Small Molecules for Highly Efficient Solution-Processed Organic Solar Cells. *Chem-Asian J.* 2014;9(4):1045-53.

[12] Liu Y, Chen C-C, Hong Z, Gao J, Yang Y, Zhou H, et al. Solution-processed small-molecule solar cells: breaking the 10% power conversion efficiency. *Sci Rep.* 2013;3.

[13] Payne MM, Parkin SR, Anthony JE, Kuo C-C, Jackson TN. Organic Field-Effect Transistors from Solution-Deposited Functionalized Acenes with Mobilities as High as  $1 \text{ cm}^2/\text{V}\cdot\text{s}$ . *J Am Chem Soc.* 2005;127(14):4986-7.

[14] Kim C, Huang P-Y, Jhuang J-W, Chen M-C, Ho J-C, Hu T-S, et al. Novel soluble pentacene and anthradithiophene derivatives for organic thin-film transistors. *Org Electron.* 2010;11(8):1363-75.

[15] Laquindanum JG, Katz HE, Lovinger AJ. Synthesis, Morphology, and Field-Effect Mobility of Anthradithiophenes. *J Am Chem Soc.* 1998;120(4):664-72.

[16] Payne MM, Odom SA, Parkin SR, Anthony JE. Stable, Crystalline Acenedithiophenes with up to Seven Linearly Fused Rings. *Org Lett.* 2004;6(19):3325-8.

[17] An TK, Park SM, Nam S, Hwang J, Yoo SJ, Lee MJ, et al. Thin Film Morphology Control via a Mixed Solvent System for High-Performance Organic Thin Film Transistors. *Sci Adv Mater.* 2013;5(9):1323-7.

[18] Kumar B, Kaushik BK, Negi YS. Organic Thin Film Transistors: Structures, Models, Materials, Fabrication, and Applications: A Review. *Polym Rev.* 2014;54(1):33-111.

[19] Choi D, An TK, Kim YJ, Chung DS, Kim SH, Park CE. Effects of semiconductor/dielectric interfacial properties on the electrical performance of top-gate organic transistors. *Org Electron.* 2014;15(7):1299-305.

[20] Chang J-F, Sun B, Breiby DW, Nielsen MM, Sölling TI, Giles M, et al. Enhanced Mobility of Poly(3-hexylthiophene) Transistors by Spin-Coating from High-Boiling-Point Solvents. *Chem Mater.* 2004;16(23):4772-6.

[21] Chae GJ, Jeong S-H, Baek JH, Walker B, Song CK, Seo JH. Improved performance in TIPS-pentacene field effect transistors using solvent additives. *J Mater Chem C.* 2013;1(27):4216-21.

[22] Umeda T, Kumaki D, Tokito S. Surface-energy-dependent field-effect mobilities up to  $1 \text{ cm}^2/\text{V s}$  for polymer thin-film transistor. *J Appl Phys.* 2009;105(2):024516.

[23] Wang C, Dong H, Hu W, Liu Y, Zhu D. Semiconducting  $\pi$ -conjugated systems in field-effect transistors: A material odyssey of organic electronics. *Chem Rev.* 2012;112(4):2208-67.

[24] Sinha S, Wang CH, Mukherjee M, Yang YW. The effect of gate dielectric modification

and film deposition temperature on the field effect mobility of copper (II) phthalocyanine thin-film transistors. *J Phys D: Appl Phys.* 2014;47(24):245103.

[25] Horii Y, Ikawa M, Sakaguchi K, Chikamatsu M, Yoshida Y, Azumi R, et al. Investigation of self-assembled monolayer treatment on SiO<sub>2</sub> gate insulator of poly(3-hexylthiophene) thin-film transistors. *Thin Solid Films.* 2009;518(2):642-6.

[26] Kim DH, Lee HS, Yang H, Yang L, Cho K. Tunable Crystal Nanostructures of Pentacene Thin Films on Gate Dielectrics Possessing Surface-Order Control. *Adv Funct Mater.* 2008;18(9):1363-70.

[27] Lee HS, Kim DH, Cho JH, Hwang M, Jang Y, Cho K. Effect of the Phase States of Self-Assembled Monolayers on Pentacene Growth and Thin-Film Transistor Characteristics. *J Am Chem Soc.* 2008;130(32):10556-64.

[28] Don Park Y, Lim JA, Lee HS, Cho K. Interface engineering in organic transistors. *Mater Today.* 2007;10(3):46-54.

[29] Mennicke U, Salditt T. Preparation of Solid-Supported Lipid Bilayers by Spin-Coating. *Langmuir.* 2002;18(21):8172-7.

[30] Katritzky AR, Mu L, Lobanov VS, Karelson M. Correlation of boiling points with molecular structure. 1. A training set of 298 diverse organics and a test set of 9 simple inorganics. *J Phys Chem.* 1996;100(24):10400-7.

[31] Grigoras S. A structural approach to calculate physical properties of pure organic substances: The critical temperature, critical volume and related properties. *J Comput Chem.* 1990;11(4):493-510.

[32] Park SH, Lee HS, Kim J-D, Breiby DW, Kim E, Park YD, et al. A polymer brush organic interlayer improves the overlying pentacene nanostructure and organic field-effect transistor performance. *J Mater Chem.* 2011;21(39):15580-6.

[33] Kim SH, Jang M, Yang H, Anthony JE, Park CE. Physicochemically Stable Polymer-Coupled Oxide Dielectrics for Multipurpose Organic Electronic Applications. *Adv Funct Mater.* 2011;21(12):2198-207.

[34] Chung DS, Lee SJ, Park JW, Choi DB, Lee DH, Park Jw, et al. High Performance Amorphous Polymeric Thin-Film Transistors Based on Poly[(1,2-bis-(2'-thienyl)vinyl-5',5'-diyl)-alt-(9,9-dioctylfluorene-2,7-diyl)] Semiconductors. *Chem Mater.* 2008;20(10):3450-6.

[35] Yin C-R, Ye S-H, Zhao J, Yi M-D, Xie L-H, Lin Z-Q, et al. Hindrance-Functionalized  $\pi$ -Stacked Polymer Host Materials of the Cardo-Type Carbazole-Fluorene Hybrid for Solution-

- Processable Blue Electrophosphorescent Devices. *Macromolecules*. 2011;44(12):4589-95.
- [36] Cho MJ, Lim JH, Hong CS, Kim JH, Lee HS, Choi DH. A tricyanopyrroline-based nonlinear optical chromophore bearing a lateral moiety: A novel steric technique for enhancing the electro-optic effect. *Dyes Pigm*. 2008;79(2):193-9.
- [37] An TK, Hahn SH, Nam S, Cha H, Rho Y, Chung DS, et al. Molecular aggregation-performance relationship in the design of novel cyclohexylethynyl end-capped quaterthiophenes for solution-processed organic transistors. *Dyes Pigm*. 2013;96(3):756-62.
- [38] Lee TW, Lee DH, Shin J, Cho MJ, Choi DH. Naphthodithiophene-Diketopyrrolopyrrole-Based donor-Acceptor alternating  $\pi$ -Conjugated polymers for Organic thin-Film transistors. *J Polym Sci, Part A: Polym Chem*. 2013;51(24):5280-90.
- [39] An TK, Jang SH, Kim SO, Jang J, Hwang J, Cha H, et al. Synthesis and Transistor Properties of Asymmetric Oligothiophenes: Relationship between Molecular Structure and Device Performance. *Chem Eur J*. 2013;19(42):14052-60.
- [40] Yum S, An TK, Wang X, Lee W, Uddin MA, Kim YJ, et al. Benzotriazole-Containing Planar Conjugated Polymers with Noncovalent Conformational Locks for Thermally Stable and Efficient Polymer Field-Effect Transistors. *Chem Mater*. 2014;26(6):2147-54.
- [41] Jang J, Park J, Nam S, Anthony JE, Kim Y, Kim KS, et al. Self-organizing properties of triethylsilylethynyl-anthradithiophene on monolayer graphene electrodes in solution-processed transistors. *Nanoscale*. 2013;5(22):11094-101.
- [42] Jones C, Boudinet D, Xia Y, Denti M, Das A, Facchetti A, et al. Synthesis and Properties of Semiconducting Bispyrroloothiophenes for Organic Field-Effect Transistors. *Chem Eur J*. 2014;20(20):5938-45.
- [43] Jeong H-G, Khim D, Jung E, Yun J-M, Kim J, Ku J, et al. Synthesis and characterization of a novel ambipolar polymer semiconductor based on a fumaronitrile core as an electron-withdrawing group. *J Polym Sci, Part A: Polym Chem*. 2013;51(5):1029-39.
- [44] Lam KH, Foong TRB, Zhang J, Grimsdale AC, Lam YM. Carboxylic acid mediated self-assembly of small molecules for organic thin film transistors. *Org Electron*. 2014;15(7):1592-7.
- [45] An TK, Kang I, Yun H-j, Cha H, Hwang J, Park S, et al. Solvent Additive to Achieve Highly Ordered Nanostructural Semicrystalline DPP Copolymers: Toward a High Charge Carrier Mobility. *Adv Mater*. 2013;25(48):7003-9.
- [46] Noh YH, Young Park S, Seo S-M, Lee HH. Root cause of hysteresis in organic thin film transistor with polymer dielectric. *Org Electron*. 2006;7(5):271-5.

[47] Lee WH, Choi HH, Kim DH, Cho K. 25th Anniversary Article: Microstructure Dependent Bias Stability of Organic Transistors. *Adv Mater.* 2014;26(11):1660-80.

[48] Shun-Wei L, Wei-Cheng S, Chih-Chien L, Wei-Lun W, Je-Min W, Yu-Hsuan H, et al. Characterization of intrinsic hysteresis of pentacene-based organic thin-film transistor through in-situ electrical measurement. *Proc Active-Matrix Flatpanel Displays and Devices (AM-FPD), 2013 Twentieth International Workshop on 2013.* 137-40.

**Table 1.** Summary of the physical properties of DPPEADT and DFEADT.

	<b>Solution (nm)</b>	<b>Film (nm)</b>	<b>HOMO (eV)</b>	<b>LUMO (eV)</b>	<b>Band gap (eV)</b>
<b>DPPEADT</b>	529, 570	543, 652	-5.18	-3.11	2.07
<b>DFEADT</b>	539, 578	559, 604	-5.22	-3.19	2.03

\* The solution of materials were  $10^{-5}$  M in chloroform.

\* HOMO-LUMO gap ( $E_g$ ) measured according to the onset of UV absorption ( $E_g = 1240/\lambda_{\text{onset}}$  eV).

\* HOMO (eV) measured according to the onset of oxidation (HOMO = 4.43 +  $E_{\text{onset}}$  )

**Table 2.** Device Performance of Solution-Processed OFETs based on DPPEADT and DFEADT

Conditions		Mobility ( $\text{cm}^2/\text{V}\cdot\text{s}$ )	$I_{on}/I_{off}$	$V_{th}$ (V)	SS (V/decade)
<b>DPPEADT</b>	CB	0.018	$6.1 \times 10^5$	-7.39	1.4
	DCB	0.079	$1.5 \times 10^6$	-1.36	0.82
	TCB	0.16	$3.1 \times 10^7$	-1.52	0.62
<b>DFEADT</b>	CB	$3.9 \times 10^{-6}$	$4.4 \times 10^2$	10	1.1
	DCB	$3.8 \times 10^{-6}$	$1.7 \times 10^2$	8.2	0.92
	TCB	$3.7 \times 10^{-6}$	$2.3 \times 10^2$	11	1.0

Scheme 1. Synthetic schemes describing the synthesis of DPPEADT and DFEADT.

**Figure 1.** UV-Vis absorption spectra of (a) DPPEADT and (b) DFEADT in solutions or the film state.

**Figure 2.** 1D XRD patterns (out-of-plane) of (a) DPPEADT and (c) DFEADT, and (in-plane) of (b) DPPEADT and (d) DFEADT annealed films.

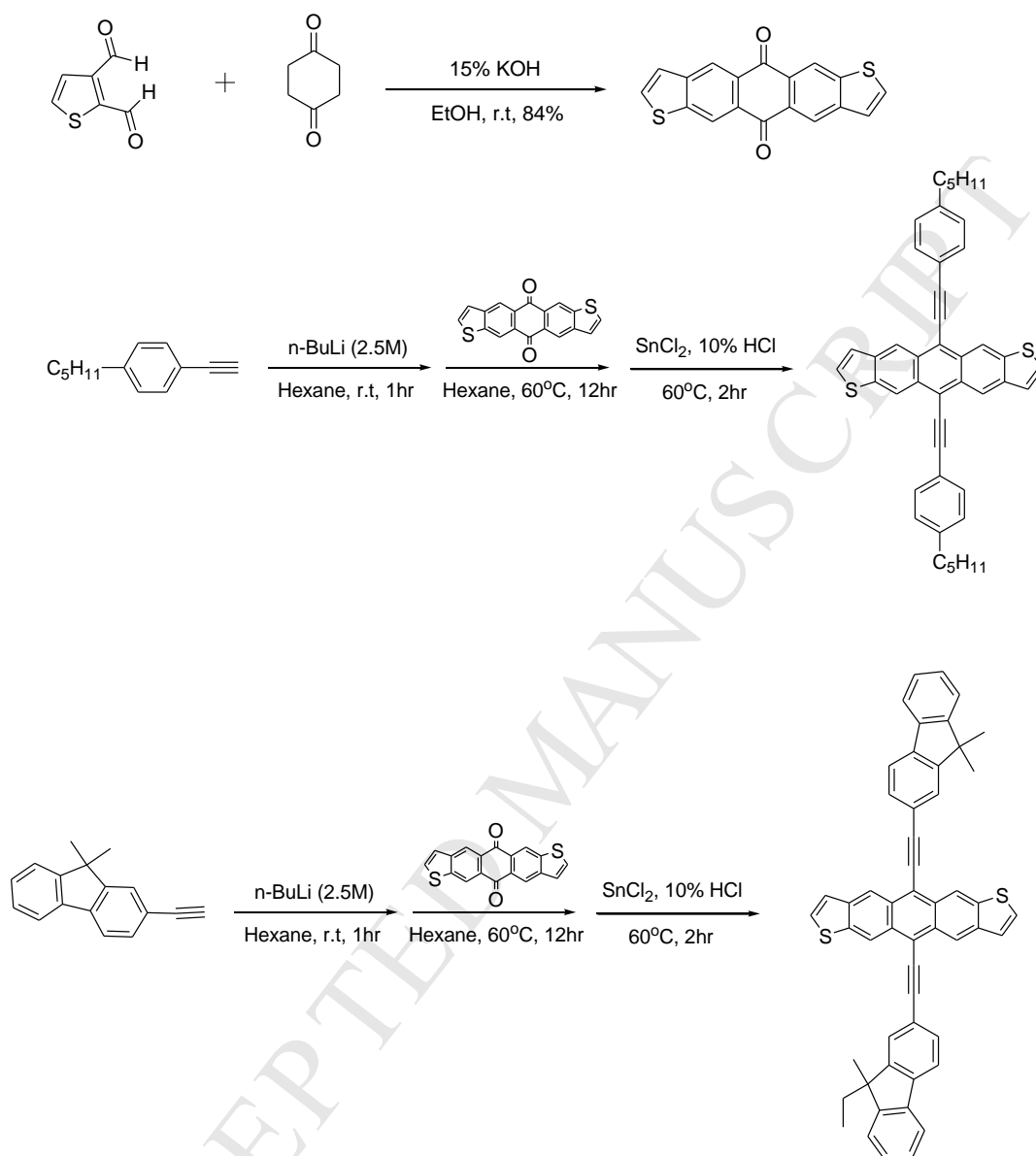
**Figure 3.** Estimated packing structures for DPPEADT.

**Figure 4.** Height-mode AFM images of DPPEADT made by (a) CB, (b) DCB and (c) TCB, and AFM images of DFEADT made by (d) CB, (e) DCB and (f) TCB. The vertical scales in (a-c) and (d-f) represent 30 and 10, respectively.

**Figure 5.** Schematic diagram of the top-contact-electrode OFETs investigated in this study.

**Figure 6.** Transfer characteristics of (a) DPPEADT and (b) DFEADT-based OFET devices measured in ambient condition.

**Figure 7.** Transfer characteristics of DPPEADT-based OFETS prepared from (a) CB, (b) DCB and (c) TCB measured in N<sub>2</sub> condition.



Scheme 1.

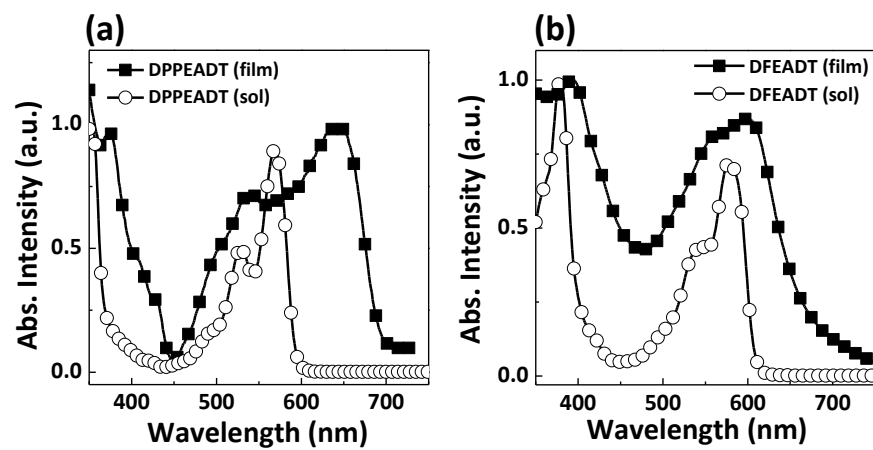


Figure 1.

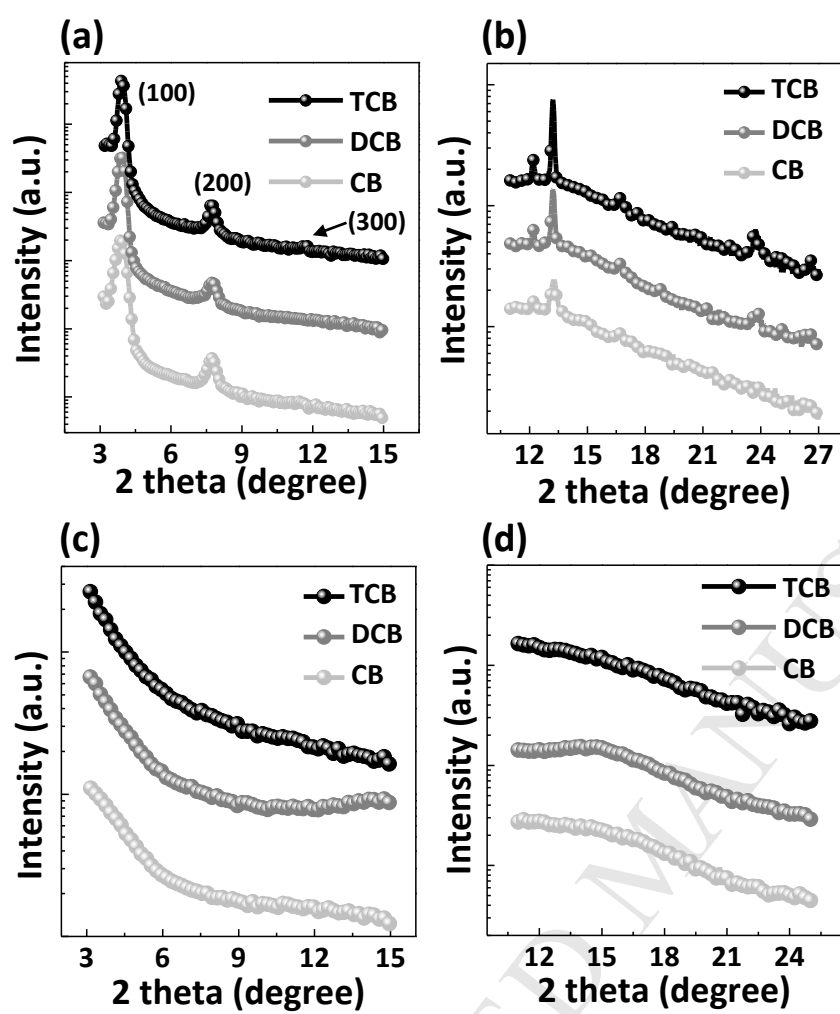


Figure 2.

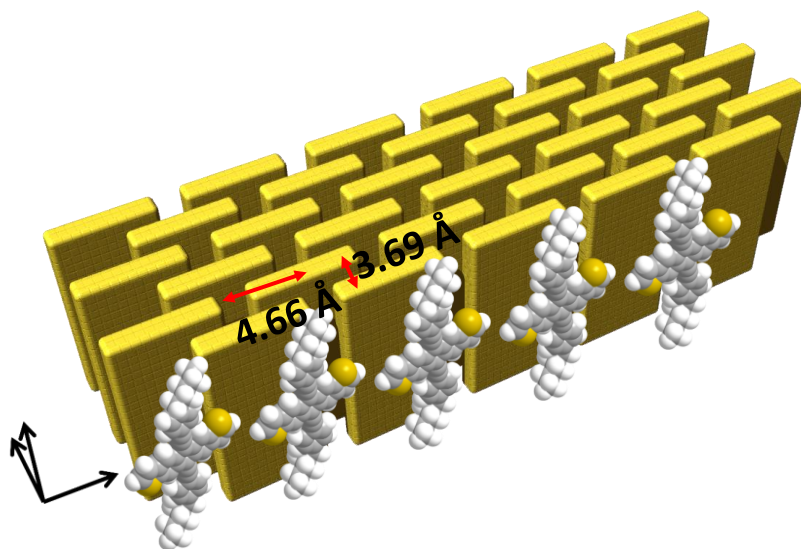


Figure 3.

ACCEPTED MANUSCRIPT

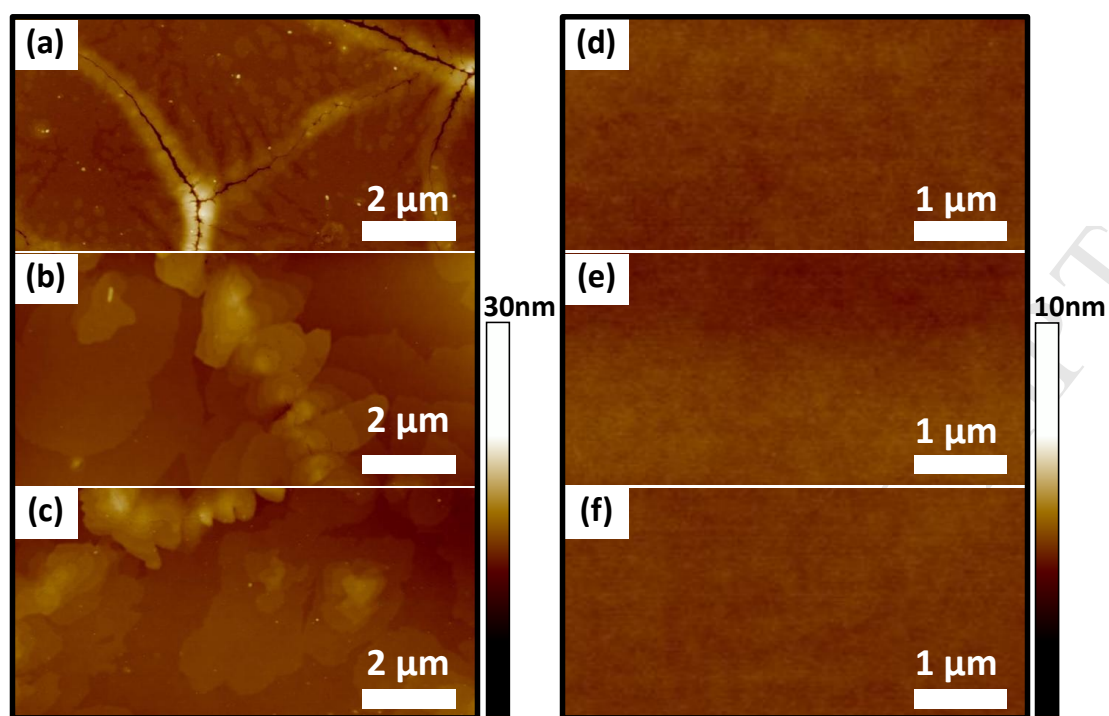


Figure 4.

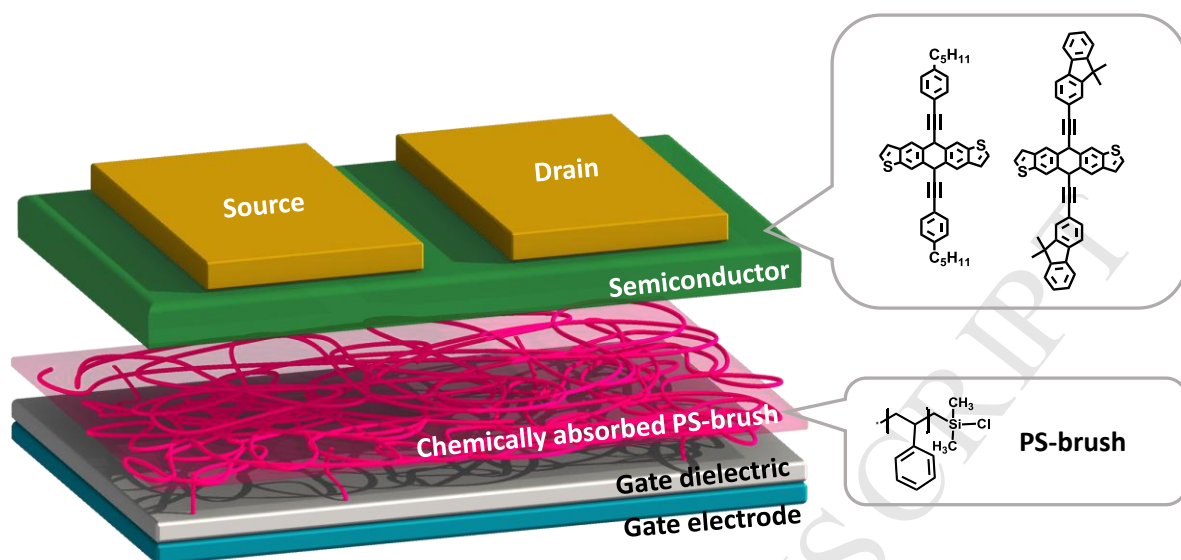


Figure 5.

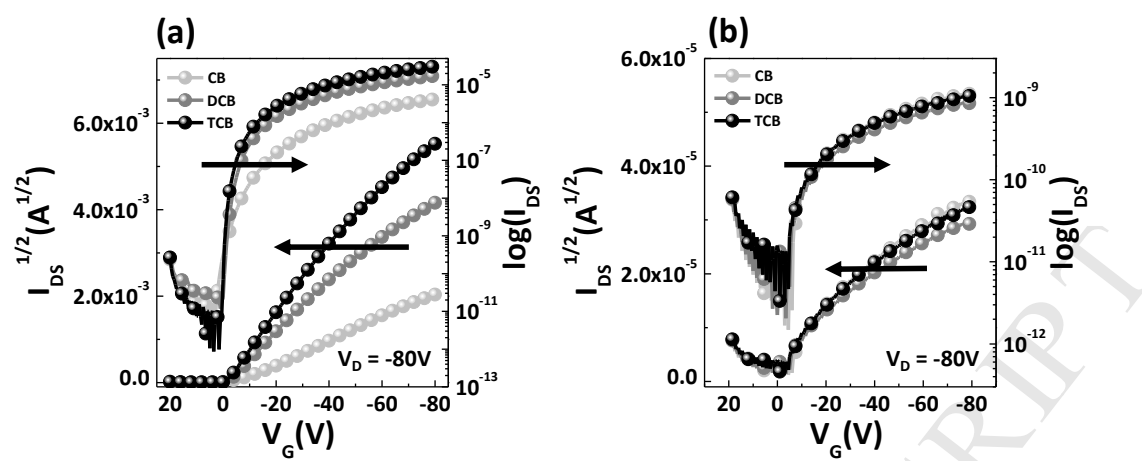


Figure 6.

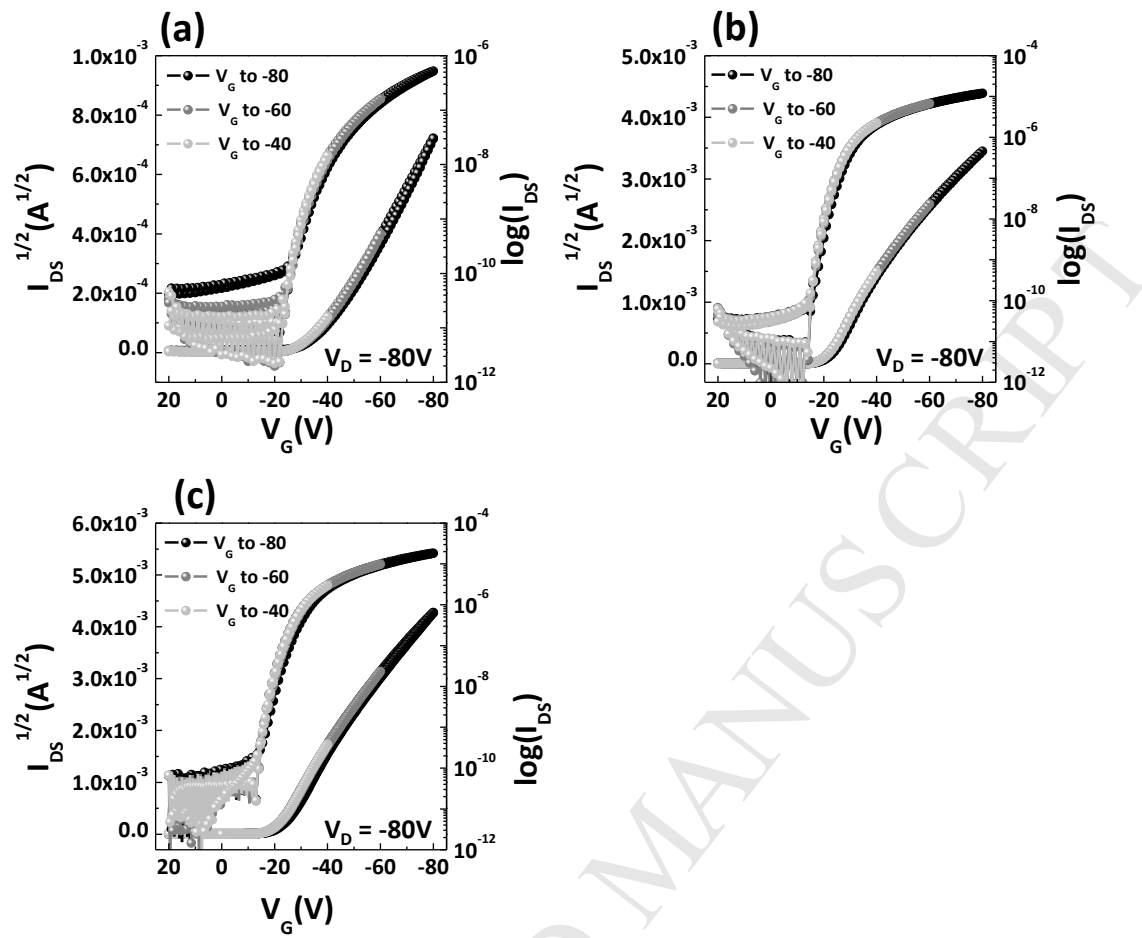


Figure 7.

Supporting Information

## **Solvent Boiling Point affects the Crystalline Properties and Performances of Anthradithiophene-based Devices**

Tae Kyu An,<sup>a</sup> Seong Jong Park,<sup>b</sup> Eun Soo Ahn,<sup>b</sup> Sang Hun Jang,<sup>c</sup> Yebyeol Kim,<sup>a</sup> Kyunghun Kim,<sup>a</sup> Hyojung Cha,<sup>a</sup> Yu Jin Kim,<sup>a</sup> Se Hyun Kim,<sup>d</sup> Chan Eon Park,<sup>\*a</sup> and Yun-Hi Kim<sup>\*b</sup>

**Figure S1.** DFT calculation using Gaussian for DPPEADT and DFEADT

**Figure S2.** Calculated length of the DPPEADT and DFEADT molecule

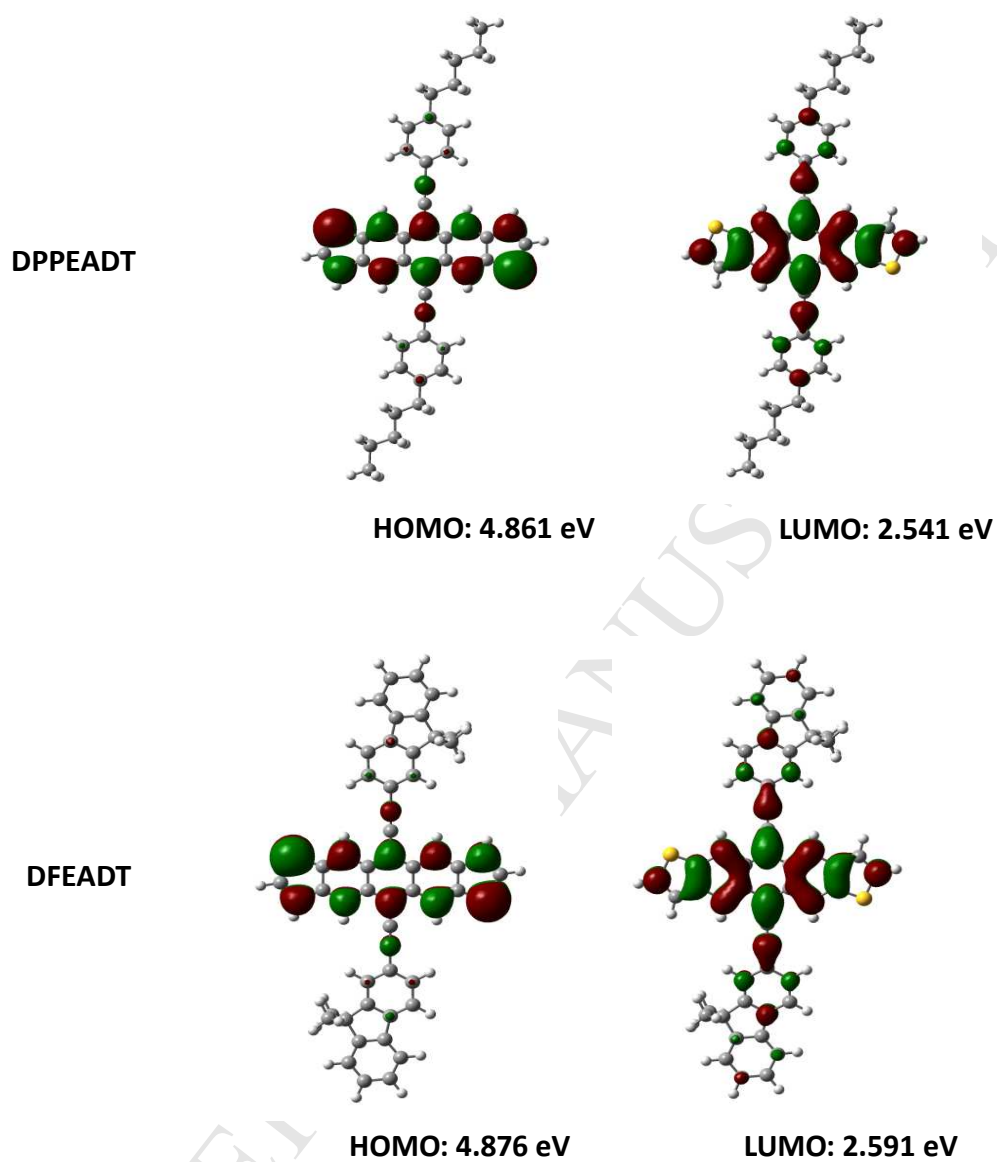


Figure S1.

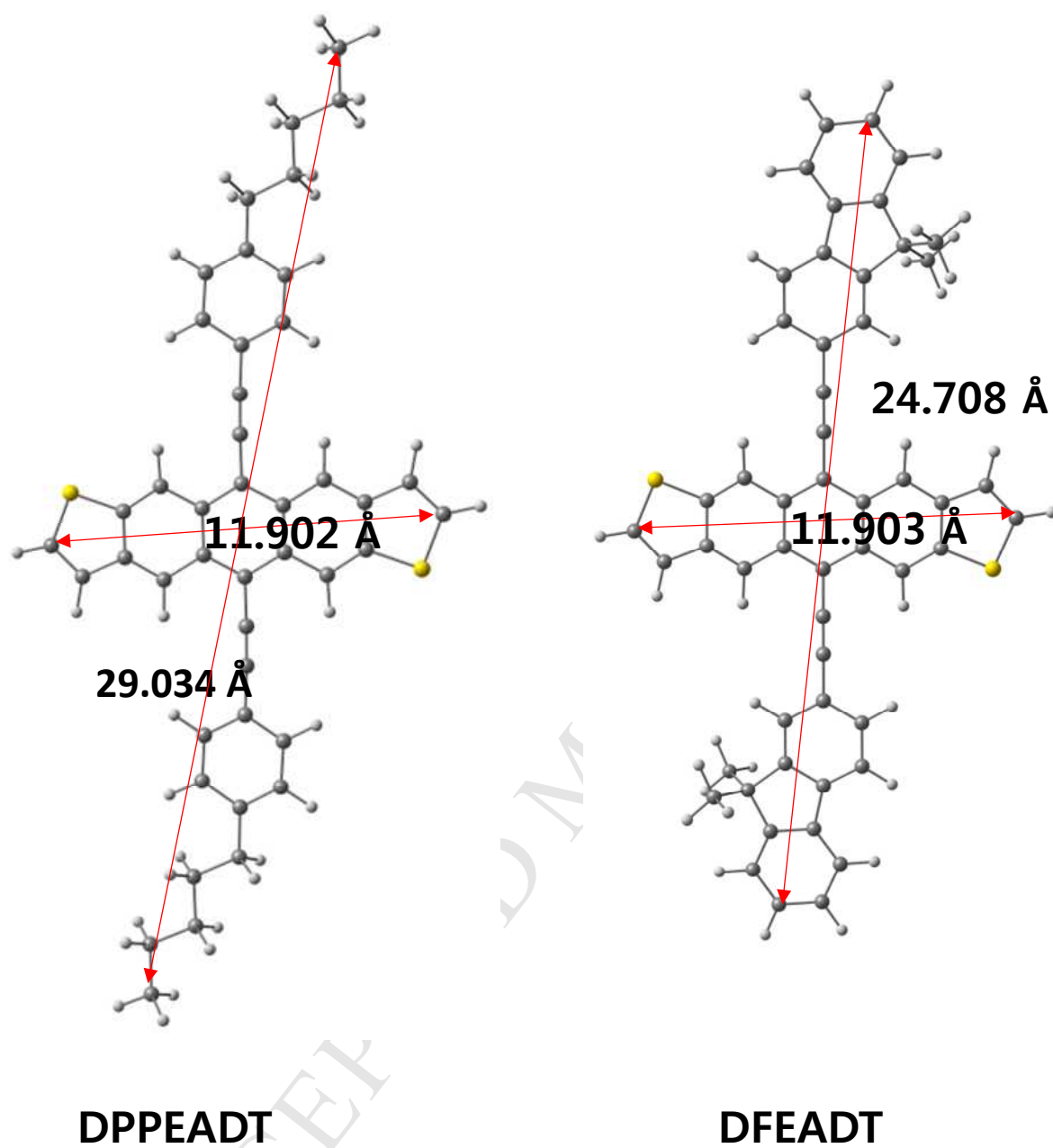


Figure S2.